Supporting information

Conceptual design and techno-economic analysis of a coal to methanol and ethylene glycol co-generation process with low carbon emission and high efficiency

Jianjun Chen[†], Yu Qian[†,‡], Siyu Yang[†,‡,*]

[†] *School of Chemical Engineering, South China University of Technology, Guangzhou 510640, China*

[‡] *Guangdong Key Laboratory of Green Chemical Products Technology, South China University of Technology, Guangzhou, 510640, PR China*

S1 Process modeling and simulation

Gasification unit

Coal is mixed with water to obtain coal slurry and then sent to the gasifier with pure oxygen. In the gasifier, raw coal quickly decomposes to form char and volatile components according to Eq. (S1)[1] at the temperature of 1350 °C.

$$\begin{aligned} C_aH_bO_cN_dS_e\ \text{(daf coal)} \rightarrow\ & x_{dev,char}C\ \text{(daf char)} + x_{dev,CH_4}CH_4 + x_{dev,C_2H_6}C_2H_6 \\ & + x_{dev,CO}CO + x_{dev,CO_2}CO_2 + x_{dev,C_6H_6}C_6H_6 + x_{dev,H_2}H_2 \\ & + x_{dev,H_2O}H_2O + x_{dev,NH_3}NH_3 + x_{dev,H_2S}H_2S \end{aligned} \quad \text{(S1)}$$

After that, a sequence of chemical reactions takes place among char, volatile component, oxygen and water,[2] as shown in **Table S1** and **Table S2**. The crude syngas is obtained through these complex reactions and then quenched with the cooling water.[3] The slag is separated from the syngas in the quench chamber. After the quenching process, the syngas is cooled down to 240 °C and sent out from the quench chamber.[4] The syngas is further cooled to 40 °C in the water scrubber and fed to the WGS unit. The scouring black water is then introduced to the flash system for recovery.

Table S1. Heterogeneous reactions in the gasification process

Solid phase Reaction	ΔH(KJ/mol)	Reaction constant
$C+\frac{1}{\Phi}O_2 \rightarrow (2-\frac{2}{\Phi})CO+(\frac{2}{\Phi}-1)CO_2$	-110.5	$k_1 = 2.363\times10^{1}\exp\left(-\frac{130000}{RT}\right)$
$C+CO_2 \rightarrow 2CO$	172.5	$k_2 = 1.127\times10^{-1}\exp\left(-\frac{140000}{RT}\right)$
$C+H_2O \rightarrow CO+H_2$	131.3	$k_3 = 2.340\times10^{1}\exp\left(-\frac{214000}{RT}\right)$
$C+2H_2 \rightarrow CH_4$	74.6	$k_4 = 5.692\times10^{-3}\exp\left(-\frac{138000}{RT}\right)$

Wherein

$$\Phi=\begin{cases} \dfrac{2Z+2}{Z+2} & d_p \le 0.005\text{cm} \\ \dfrac{(2Z+2)-Z(d_p-0.005)/0.095}{Z+2} & 0.005\text{cm} \le d_p \le 0.1\text{cm} \\ 1.0 & d_p > 0.1\text{cm} \end{cases}$$

$$Z=\frac{[CO]}{[CO_2]}=2500e^{\frac{-6249}{T}}$$

Table S2. Homogeneous reactions in the gasification process

Gaseous phase Reaction	$\Delta H(KJ/mol)$	Reaction constant
$H_2+\frac{1}{2}O_2 \rightarrow H_2O$	-242	$k_1=1\times10^{11}\exp\left(-\frac{420000}{RT}\right)$
$CH_4+\frac{1}{2}O_2 \rightarrow CO+2H_2$	35.5	$k_2=2.47\times10^{9}\exp\left(-\frac{125.6}{RT}\right)$
$CO+\frac{1}{2}O_2 \rightarrow CO_2$	283.1	$k_3=1.26\times10^{10}\exp\left(-\frac{167000}{RT}\right)$
$C_2H_6+O_2 \rightarrow 2CO+3H_2$	-120.6	$k_4=1\times10^{8}$
$C_6H_6+3O_2 \rightarrow 6CO+3H_2$	-124.3	$k_4=1\times10^{8}$
$CO+H_2O \rightarrow CO_2+H_2$	-41.2	$k_4=2.78\times10^{-3}\exp\left(-\frac{12560}{RT}\right)$
$CH_4+H_2O \rightarrow CO+3H_2$	205.9	$k_4=3\times10^{5}\exp\left(-\frac{125.6}{RT}\right)$

Process simulation flowsheet of the gasification unit is illustrated in **Figure S1**. The PR-BM method is selected to estimate the physical properties of the gasification process. A RYield model is used for modeling the coal decomposition stage while the combustion and gasification stage are modeled in an RGibbs block based on Gibbs free energy minimization principle.[5] The temperature and pressure for the gasification are determined to be 1350 °C and 6.4 MPa according to literature.[4]

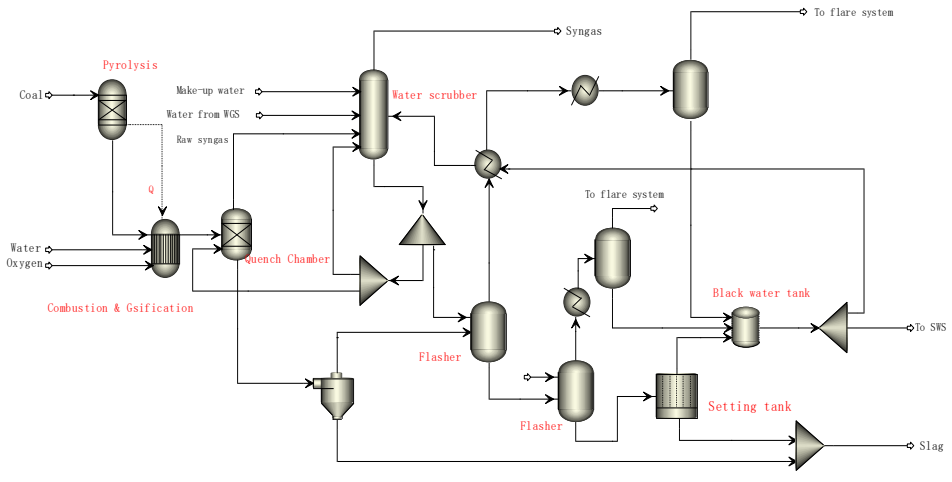

Figure S1. Process flowsheet of gasification unit

Table S3 shows the comparison of simulation results with the literature data. It is shown that the gasification model generally agrees with the reference data.

Table S3. Verification of simulation results for coal gasification unit

Source	Temperature	Pressure	Mole composition (%)							
	(°C)	(bar)	CO	H_2	CO_2	H_2S	H_2O	NH_3	N_2	Ar
Simulation results	240	64	21.52	13.97	6.12	0.12	57.58	0.31	0.38	-
Reference data[3]	241	64	21.37	14.01	6.15	0.16	57.31	-	0.46	0.54

Water gas shift unit

Water gas shift unit is used to adjust the H_2/CO of the syngas. The main reaction in WGS reactor is shown in Eq. (2) and the reaction takes place under the temperature of 483 °C. The process simulation flowsheet of WGS unit is displayed in **Figure S2** and the SRK property method is chosen for simulation.[5] The crude syngas from the gasifier is separated into two parts. One part of the syngas is sent to the shift reactor for shifting reaction, modelled by the stoichiometry reactors (RStoic model), and then mixed with the unshifted syngas. The heat produced in the reaction is recovered with a series of heat exchangers and flashers, which is modelled by HeatX model and Flash model.[6,7] The syngas is finally cooled to 40 °C and fed to the following AGR unit for CO_2 and H_2S gases removal.

$$CO + H_2O \rightarrow CO_2 + H_2 \qquad \Delta H = -41.2\ kJ/mol \qquad (S2)$$

The verification of simulation results for WGS unit is shown in **Table S4**. As can be seen, the results are similar to the reference data. The slight gap may be resulted from the small difference in shift ratio.

Table S4. Verification of simulation results for WGS unit

Source	Temperature	Pressure	Mole composition (%)							
	(°C)	(bar)	CO	H_2	CO_2	H_2S	H_2O	NH_3	N_2	Ar
Simulation results	40	60	20.12	45.97	32.12	0.28	0.12	0.41	0.98	-
Reference data[3]	40	60	19.91	46.27	31.52	0.30	0.15	-	0.86	1.01

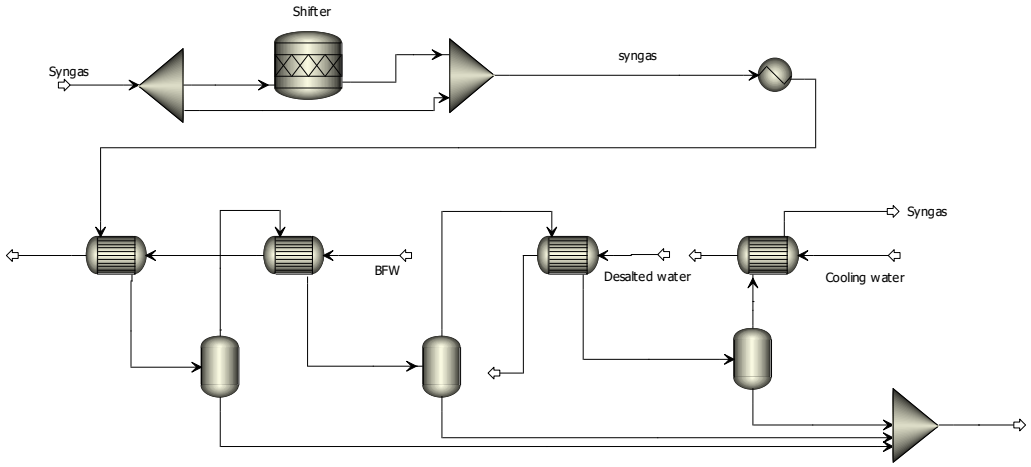

Figure S2. Process flowsheet of WGS unit

Acid gas removal unit

In this paper, the mature industrialized Rectisol process is selected for acid gas removal.[8] The process simulation flowsheet of AGR unit is presented in **Figure S3**. The syngas from the WGS unit, together with the recycling gas, is mixed with small amount of chilling methanol to keep off water freezing. Then the mingled syngas is colled down to -20 ^{o}C and sent to the flash tank to separate the liquid methanol-water mixture. After that, the syngas enters the bottom of the Rectisol absorber T101. Methanol at the temperature of -50 ^{o}C is used as the adsorbent and goes from the top of the absorber. The removal of CO_2 and H_2 can be achieved in one tower by the Rectisol process at the same time. In the upside of the absorber, CO_2 is removed from the top of the absorber. Meanwhile, the temperature of solvent increases with the adsorption of CO_2, which decrease the absorption ability of methanol. Thus, the absorption column is equipped with the side cooling exchangers to maintain the high absorption ability.

The purified syngas is obtained at the top of the absorber after absorption, which is available for gas separation and methanol synthesis processes. In the downside of the absorber, H_2S is further removed by the CO_2-rich methanol from the middle of the tower as H_2S has a higher solubility in chilling methanol than CO_2. The resulted CO_2-rich methanol and H_2S/CO_2-rich methanol are then obtained at the downside of the

absorber for further solvent recovery.

As part of the CO and H_2 is dissolved in methanol during the absorption process, the flash drum D101 and D102 is used for CO and H_2 recovery. After flashing, CO and H_2 are recycled and mixed with the raw syngas. The rich solvent from D101 is then sent to the CO_2 product column T102, and the purified CO_2 product retrived from the top of the column is sent to the carbon capture and storage system. The H_2S/CO_2-rich methanol solvent from D102 is then sent to the H_2S enrichment column T103 to desorb CO_2 by N_2 stripping. The H_2S-rich methanol is further regenerated with distillation in the methanol regeneration column T104. Finally, the lean methanol is sent to the methanol/water separation column T105, where the methanol is futher dehydrated through distillation and circulated to the top of the absorber.

For modeling the Rectisol process, PC-SAFT[9] is selected as the thermodynamic method. The absorption column, CO_2 product column, H_2S enrichment column, methanol regeneration column and methanol/water separation column are simulated with the RadFrac model. The Flash model is selected for flash drums simulation.

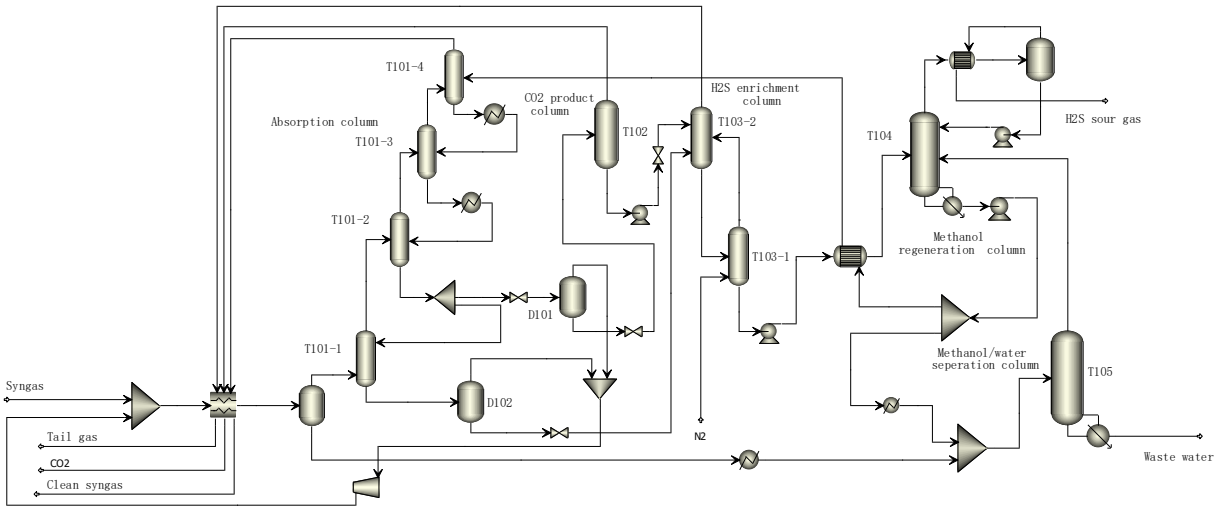

Figure S3. Process flowsheet of AGR unit

Coking unit

The process simulation flowsheet of coking unit is displayed in **Figure S4**. The blending coking coal is sent to the coking furnace with the temperature of 1100 °C.

In the coking furnace, coke is dried and goes through the thermal decomposition process to produce coke, COG, and coal tar, as shown in Eqs. (S3) - (S4).

$$\text{Coal (wet)} \rightarrow \text{coal (dry)} + 0.055H_2O \quad \text{(S3)}$$

$$\text{Coal} \rightarrow \text{coke} + \text{tar} + \text{COG} \quad \text{(S4)}$$

The yield model of the coking process is shown in Eqs. (S5) - (S11) [10]:

$$y_{\text{coke}} = 103.19 - 0.75V_{\text{coal}} - 0.0067t_J \quad \text{(S5)}$$

$$y_{\text{COG}} = 3.3\sqrt{V_{\text{coal}} - y_{\text{coke}}V_{coke}} \quad \text{(S6)}$$

$$y_{\text{tar}} = -18.36 + 1.53V_{\text{daf,coal}} - 0.026\left(V_{\text{daf,coal}}\right)^2 \quad \text{(S7)}$$

$$y_{\text{benzen}} = -1.61 + 0.144V_{\text{daf,coal}} - 0.0016\left(V_{\text{daf,coal}}\right)^2 \quad \text{(S8)}$$

$$y_{\text{amonia}} = \frac{17}{14}b^{'}N \quad \text{(S9)}$$

$$y_{\text{S}} = c^{'}S_{\text{daf}} \quad \text{(S10)}$$

$$y_{\text{H}_2\text{O}} = \frac{18}{16}a^{'}O_{\text{daf}} \quad \text{(S11)}$$

Here y_{coke}, y_{COG}, y_{tar}, y_{benzen}, y_{amonia}, y_{S}, and $y_{\text{H}_2\text{O}}$ stand for the yield of coke, COG, coal tar, crude benzenes, ammonia, sulfur and water, respectively. V_{coal} and V_{coke} denote the concentration of volatile matter of the coal and coke (wt%,dry); $V_{\text{daf,coal}}$, S_{daf}, and O_{daf} signify the content of volatile matter, sulfur and oxygen of the raw coal (wt%,dry); N is the content of nitrogen of the raw coal (wt%,dry); t_J=1100°C; $a^{'}$=0.42; $b^{'}$=0.15; $c^{'}$=0.17.

The hot coke is then cooled to 200 °C through the quenching chamber. Liquid coal tar is separated from the high temperature COG and the gas is then sent to the sulfur removal unit. PR-BM is used as the thermodynamic method in the coking

section. The RYield model is used for simulating the coking process and the yield model of the coking process is shown in Eqs. (S5)- (S11) in supporting information. The composition of COG is shown in **Table S5**.

Table S5. The composition of COG

Component	H_2	CO	CO_2	CH_4	C_2H_4	O_2	N_2
Content（V%）	58	6.2	2.2	26	2.5	0.6	4.5

Table S6 shows the comparison of the simulation results with industrial data. As can be seen, the yields of coke, COG and tar are closely in consistent to the industrial data, indicating the satisfaction of the model in estimating the coking process.

Table S6. Comparison of the simulation results and industrial data of the coking unit

	Simulation	Industrial data[10]
coke（t/h）	386	383
COG（km^3/h）	172	179
tar（t/h）	24.8	25.3

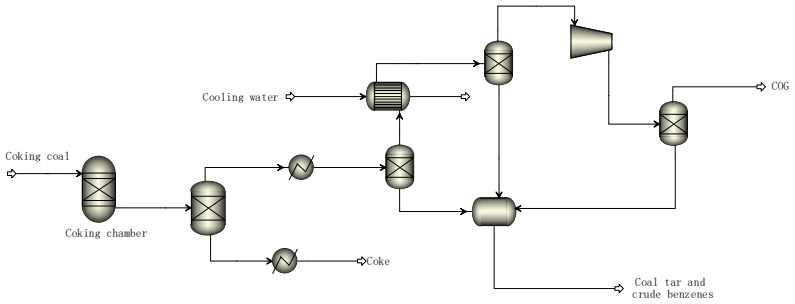

Figure S4. Process flowsheet of coking unit

MPO unit

The MPO is a mature industrial method for converting methane in the COG into effective component of syngas[11]. The MPO used in this paper is a non-catalytic reaction. The main chemical reactions occurred in this process are shown in Eqs. (S12) - (S18).[12]

$$CH_4 + 0.5O_2 \rightarrow CO + 2H_2 \qquad \Delta H = -36\ kJ/mol \qquad (S12)$$

$$2H_2 + O_2 \rightarrow 2H_2O \qquad \Delta H = -571.7\ kJ/mol \qquad (S13)$$

$$CH_4 + 2O_2 \rightarrow CO_2 + 2H_2O \qquad \Delta H = -890.4\ kJ/mol \qquad (S14)$$

$$2CH_4 + 3O_2 \rightarrow 2CO + 4H_2O \qquad \Delta H = -890.4\ kJ/mol \qquad (S15)$$

$$CH_4 + CO_2 \leftrightarrow 2CO + 2H_2 \qquad \Delta H = +247.3\ kJ/mol \qquad (S16)$$

$$CH_4 + H_2O \leftrightarrow CO + 3H_2 \qquad \Delta H = +206.1\ kJ/mol \qquad (S17)$$

$$CO_2 + H_2 \leftrightarrow CO + H_2O \qquad \Delta H = +41.2\ kJ/mol \qquad (S18)$$

As illustrated in **Figure S5**, COG is compressed to 3.9 MPa and then sent to the MPO reactor together with oxygen to generate syngas. A heat exchanger is used for the recovering of heat from the resulted hot syngas by heating the COG feedstock. The cooled syngas then sent to the methanol synthesis unit. The PR-BM method is used for estimating the physical properties of the components. The Compressor model is selected for simulation of the COG compression. The RGibbs model is chosen for modeling the MPO reaction in consideration of the thermodynamic equilibrium.

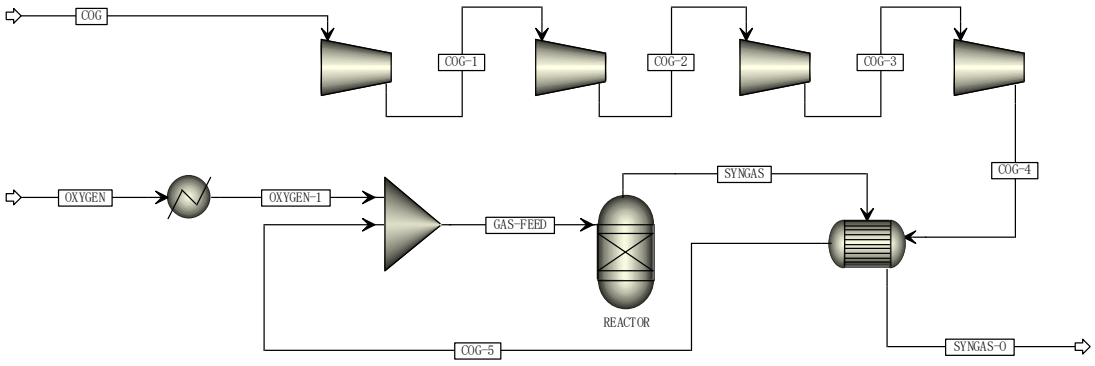

Figure S5. Process flowsheet of MPO unit

Methanol synthesis unit

The commercial Davy methanol synthesis process is used in this paper, as shown in **Figure S6**. In order to maximize the methanol conversion, two reactors are configured. The syngas from the first reactor is cooled to separate methanol and then

fed to the second reactor for further reaction. The main reactions occurred in the reactors are described as Eqs. (S19) -(S21). The $Cu/ZnO/Al_2O_3$ catalyst is used for the methanol synthesis.[13] The unreacted syngas is separated from the products and recycled to the first reactor to increase the methanol productivity. The crude methanol is then refined via distillation. The Peng-Rob method is chosen for estimating the thermodynamic properties of the components. The RPlug model is used for the simulation of methanol synthesis and the separation columns are simulated by RadFrac model in Aspen plus[14].

$$CO + 2H_2 \rightarrow CH_3OH \qquad \Delta H = -90.55\ \text{kJ/mol} \qquad (S19)$$

$$CO_2 + 3H_2 \rightarrow CH_3OH + H_2O \qquad \Delta H = -49.43\ \text{kJ/mol} \qquad (S20)$$

$$CO_2 + H_2 \rightarrow CO + H_2O \qquad \Delta H = +41.2\ \text{kJ/mol} \qquad (S21)$$

The related kinetic equation of methanol synthesis reactions is described as follows:

$$r_{MeOH} = \frac{k_1 p_{CO_2} p_{H_2} \left(1 - \frac{1}{K_1^{eq}} \frac{p_{H_2O} p_{CH_3OH}}{p_{H_2}^3 p_{CO_2}}\right)}{\left(1 + K_1 \frac{p_{H_2O}}{p_{H_2}} + K_2 \sqrt{p_{H_2}} + K_3 p_{H_2O}\right)^3} \qquad (S22)$$

$$r_{RWGS} = \frac{k_2 p_{CO_2} \left(1 - \frac{1}{K_2^{eq}} \frac{p_{H_2O} p_{CO}}{p_{H_2} p_{CO_2}}\right)}{\left(1 + K_1 \frac{p_{H_2O}}{p_{H_2}} + K_2 \sqrt{p_{H_2}} + K_3 p_{H_2O}\right)} \qquad (S23)$$

Here, k_1 and k_2 stand for the kinetic factors; K_1^{eq} and K_2^{eq} are the equilibrium constants, which can be calculated through Eqs. (S24)-A(S25):

$$\log_{10} K_1^{eq} = \frac{3066}{T} - 10.592 \quad \text{(S24)}$$

$$\log_{10} 1/K_1^{eq} = \frac{-2073}{T} - 2.029 \quad \text{(S25)}$$

K_3, K_4, K_5 are the adsorption equilibrium constants and the values are listed in **Table S7**.

Table S7. Parameter values for the methanol synthesis kinetics

$k = A \cdot e^{B/RT}$	A	B
k_1	1.07	36,696
k_2	1.22×10^{10}	−94,765
K_3	3453.38	–
K_4	0.499	17,197
K_5	6.62	6.62×10^{-11}

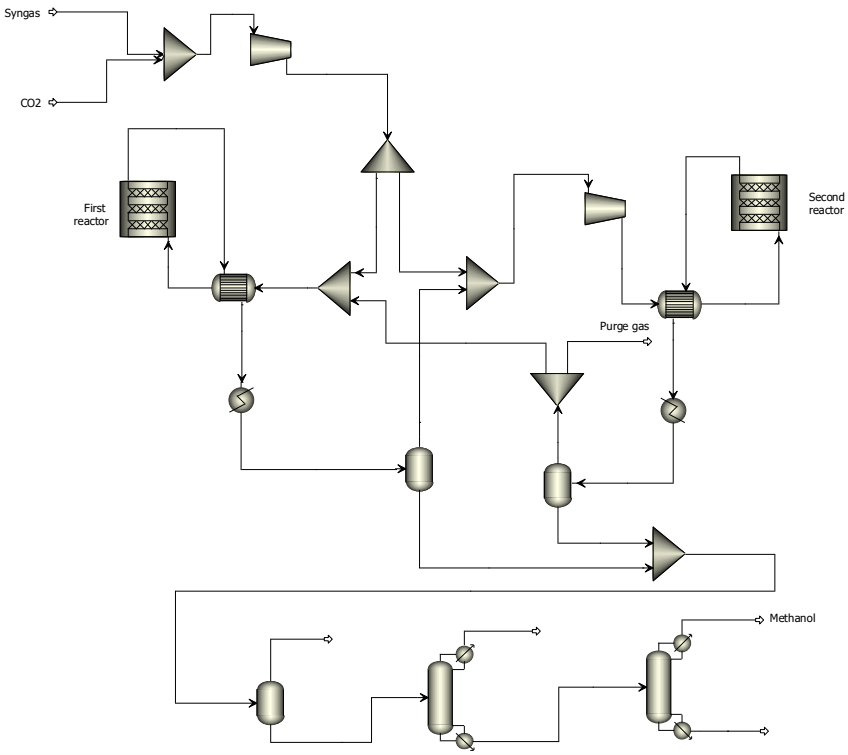

Figure S6. Process flowsheet of methanol synthesis unit

EG synthesis unit

Oxalate process route is selected for EG synthesis, which mainly includes two parts: dimethyl oxalate (DMO) synthesis and EG synthesis, as shown in **Figure S7**. During DMO synthesis reaction, methanol is reacted with NO and O_2 to obtain methyl nitrite (MN). After that, CO and MN are reacted in a DMO synthesis reactor to

generate DMO, NO, and by-product dimethyl carbonate (DMC).

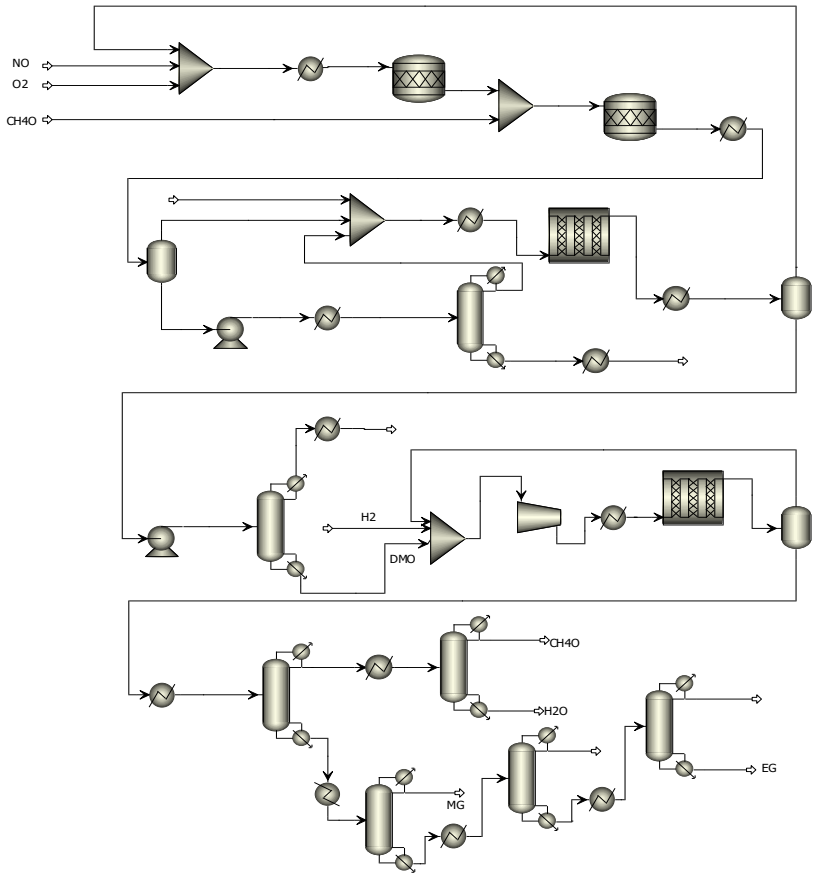

Figure S7. Process flowsheet of EG synthesis unit

The reactions involved in the DMO synthesis process are shown in Eqs. (S26)–(S29).[15]

$$2CO + 2MN \rightarrow DMO + 2NO \quad \text{(S26)}$$

$$2NO + 2CH_3OH + 0.5O_2 \rightarrow 2MN + 2H_2O \quad \text{(S27)}$$

$$CO + 2MN \rightarrow DMC + 2NO \quad \text{(S28)}$$

$$2CO + 2CH_3OH + 0.5O_2 \rightarrow DMO + 2H_2O \quad \text{(S29)}$$

In terms of the EG synthesis process, DMO is further reacted with pure H_2 to generate crude glycol on copper catalyst, and methanol is simultaneously produced. This process is mainly divided into two stages: the first stage is the hydrogenation of DMO to form methyl glycolate (MG) as an intermediate product. At the second stage,

MG is further hydrogenated to generate glycol. Besides, ethanol is also obtained as a by-product. The main and side reactions are shown in Eqs. (S30) -(S33).[16]

$$DMO + H_2 \rightarrow MG + CH_3OH \quad (S30)$$

$$MG + H_2 \rightarrow EG + CH_3OH \quad (S31)$$

$$EG + H_2 \rightarrow CH_3CH_2OH + H_2O \quad (S32)$$

$$DMO + 4H_2 \rightarrow EG + 2CH_3OH \quad (S33)$$

The RCSTR model is used to simulate the DMO synthesis, in which the temperature and pressure are 120 °C and 0.2 MPa, respectively. Rplug is used to simulate the hydrogenation of DMO reaction. The reaction temperature is 200 °C and the pressure is 3.0 MPa. The relevant kinetic equations for the DMO synthesis are shown Eqs. (S34) - (S39).[17]

$$r_{DMO} = \frac{K_a K_b p_{CO}^2 p_{MN}^2}{K_a p_{MN}^2 + K_a K_b p_{CO}^2 p_{MN}^2 / K_c + K_b p_{CO}^2} \quad (S34)$$

$$K_a = 1.46\times10^9 \exp\left(-6.895\times10^4 / RT\right) \quad (S35)$$

$$K_b = 4.1\times10^{12} \exp\left(-3.945\times10^4 / RT\right) \quad (S36)$$

$$K_c = 1.89\times105 \exp\left(-6.312\times10^4 / RT\right) \quad (S37)$$

$$r_{DMC} = 4.68 \exp\left(-\frac{0.179\times10^5}{RT}\right) P_{CO}^{0.88} P_{MN}^{0.93} P_{NO}^{-0.35} \quad (S38)$$

$$r_{MN} = 0.03815 \exp\left(-\frac{43505}{RT}\right) P_{NO}^{1} P_{O_2}^{0.1} \quad (S39)$$

The kinetics equations and parameters of EG synthesis are present in Eqs. (S40)–(S42).[18]

$$r_{MG}=\frac{k_1\left(P_{DMO}-\frac{P_{MG}P_{MeOH}}{K_{p_1}P_{H_2}^2}\right)}{\left(1+K_{EG}P_{EG}+K_{MeOH}P_{MeOH}+\frac{K_{DMO}P_{MG}P_{MeOH}}{K_{p_1}P_{H_2}^2}+\frac{K_{EG}P_{MG}P_{MeOH}}{K_{p_2}P_{H_2}^2}+K_{ET}P_{ET}\right)} \quad \text{(S40)}$$

$$r_{MG}=\frac{k_2\left(P_{MG}-\frac{P_{EG}P_{MeOH}}{K_{p_2}P_{H_2}^2}\right)}{\left(1+K_{EG}P_{EG}+K_{MeOH}P_{MeOH}+\frac{K_{DMO}P_{MG}P_{MeOH}}{K_{p_1}P_{H_2}^2}+\frac{K_{EG}P_{MG}P_{MeOH}}{K_{p_2}P_{H_2}^2}+K_{ET}P_{ET}\right)} \quad \text{(S41)}$$

$$r_{ET}=\frac{k_3P_{EG}}{\left(1+K_{EG}P_{EG}+K_{MeOH}P_{MeOH}+\frac{K_{DMO}P_{MG}P_{MeOH}}{K_{p_1}P_{H_2}^2}+\frac{K_{EG}P_{MG}P_{MeOH}}{K_{p_2}P_{H_2}^2}+K_{ET}P_{ET}\right)} \quad \text{(S42)}$$

Where r_{MG}, r_{MG}, r_{ET} represents the rate constant of the reaction, P_i represents the partial pressure of each component in the reaction. The values of K_i are listed in **Table S4**.

Table S4 Parameter values for the EG synthesis kinetics

$K_i = A\cdot e^{\frac{B}{RT}}$	*A*	*B*
k_1	3.87×10^{7}	44,284
k_2	1.75×10^{6}	37,710
k_3	8.78×10^{13}	137,380
K_{H2}	1.20×10^{-3}	8348
K_{ME}	5.49×10^{-12}	66,356
K_{EG}	1.85×10^{-4}	18,883
K_{MG}	2.65×10^{-2}	19,242
K_{DMO}	7.92×10^{-5}	118,170
K_{P1}	163.4161	17,759
K_{P2}	0.2873	15,921

S2 Chemical energy of pure components

Table S5. Chemical energy of pure components

Component	$E_{x,i}^{ch}$ (KJ/kg)	Phase
CO[19]	9,821.42	g
H_2[19]	117,120.11	g
CO_2[19]	451.49	g
CH_4[19]	51,839.57	g
N_2[19]	24.63	g
O_2[19]	124.07	g
H_2O[19]	527.34	g
H_2O[19]	49.96	l
NO[19]	2,667	g
H_2S[19]	27,608	g
S[19]	19,507.2	s
CH_4O[19]	22918.08	l
$C_2H_6O_2$[20]	19,451.23	l
C_2H_6O[20]	29,650	l
NH_3[20]	19,840.81	g
Crude benzene[21]	42,080.63	l
Coal tar[21]	40,738.59	l
Coke[21]	31,412.26	s
Coking coal[21]	32,648.56	s
Gasification Coal[21]	31,277.33	s

S3 Estimation of product cost

Table S6. Ratio factors for capital investment

Component	Ratio factor (RF, %)
(1) Direct investment	
(1.1) Equipment	21
(1.2) Installation	10
(1.3) Instruments and controls	5
(1.4) Piping	12
(1.5) Electrical	6
(1.6) Buildings (including services)	15
(1.7) Land	1
(2) Indirect investment	
(2.1) Engineering and supervision	10
(2.2) Construction expenses	9
(2.3) Contractor's fee	4
(2.4) Contingency	7
(3) Fixed-capital investment	100
(4) Working capital	17
(5) Total capital investment	117

Table S7. Assumptions for the estimation of product cost

Component	Basis
(1) Raw material cost	Coal price 58 US$/t
(2) Utilities cost	Water 0.3 US$/t, electricity 0.11 US$/kWh
(3) Operating & Maintenance	
(3.1) Operating labor	1000 operators (17,390 US$/operator/year)
(3.2) Direct supervisory and clerical labor	20 % of operating labor
(3.3) Maintenance and repairs	2 % of fixed capital investment
(3.4) Operating supplies	0.7 % of fixed capital investment
(3.5) Laboratory charge	15 % of operating labor
(4) Depreciation	Life period: 20 years, salvage value: 5%
(5) Plant overhead cost	60 % of cost for operating labor, supervision, and maintenance
(6) Administrative cost	2 % of product cost
(7) Distribution and selling cost	2 % of product cost
(8) Byproducts	Coal tar 346.8 US$/t, crude benzenes 559.5 US$/t, EG: 750 US$/t
(9) Product cost	(1) +(2) +(3) +(4) +(5) +(6) +(7)-(8)

S4 Key parameters analysis

Key parameters in MPO unit

Effect of temperature and pressure

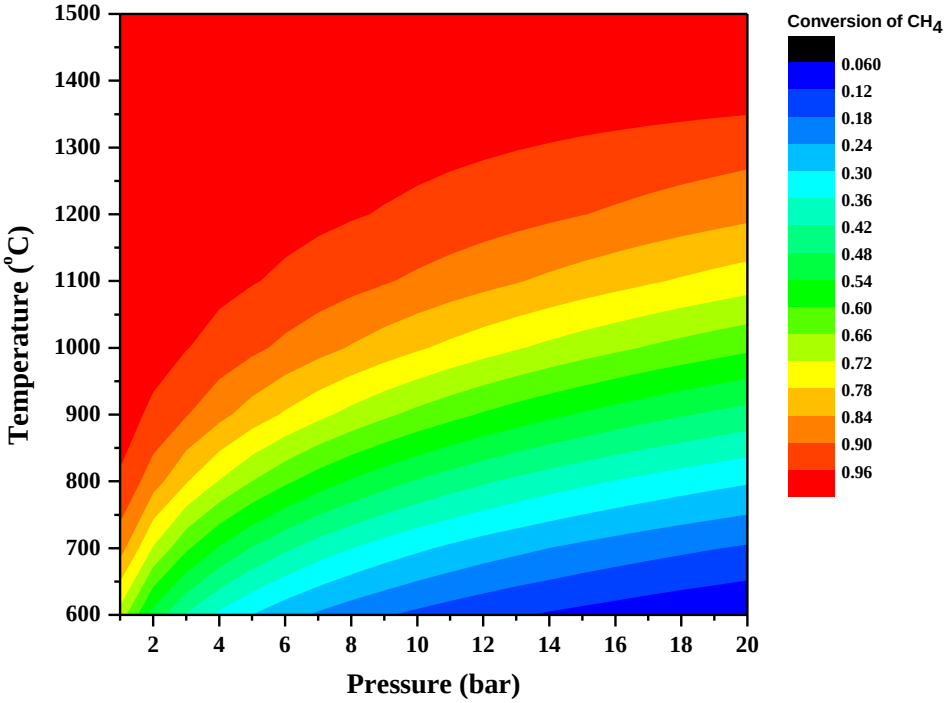

Figure S8. Effect of MPO temperature and pressure on methane conversion

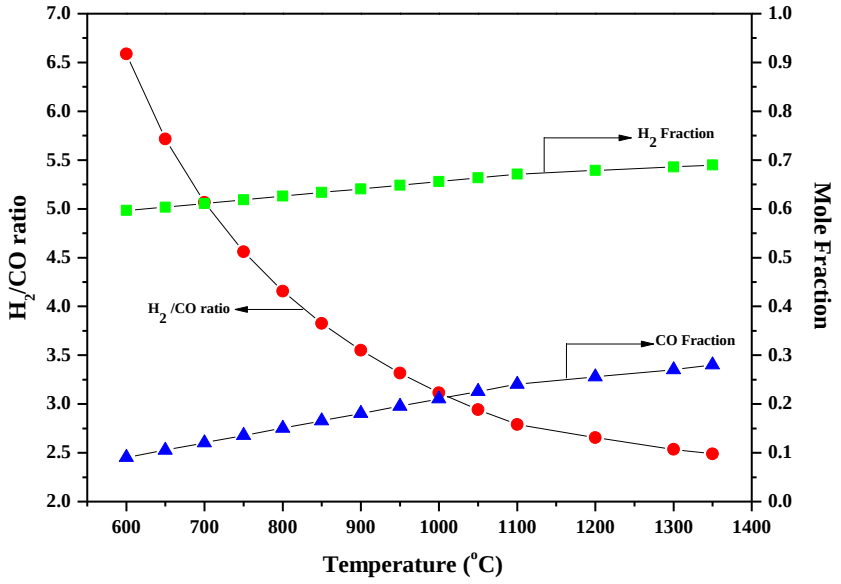

Figure S9. Effect of MPO temperature on H_2/CO

The effect of MPO temperature on the techno-economic performance of the system is shown in Figure S10. As can be seen, the carbon utilization efficiency increased from 50% to 54.1% as the temperature varied from 600 °C to 1350 °C. The GHG emissions decreased from 1.6 t CO_2-eq.$t^{-1}$to 1.58 t CO_2-eq.t^{-1}. The exergy efficiency increased from 66.6% to 68.1%. It means that the increase of MPO temperature can convert more CH_4 to product, achieving high carbon utilization efficiency and exergy efficiency, as well as low GHG emission. In term of the economic performance, the IRR was improved from 25.2% to 26%.

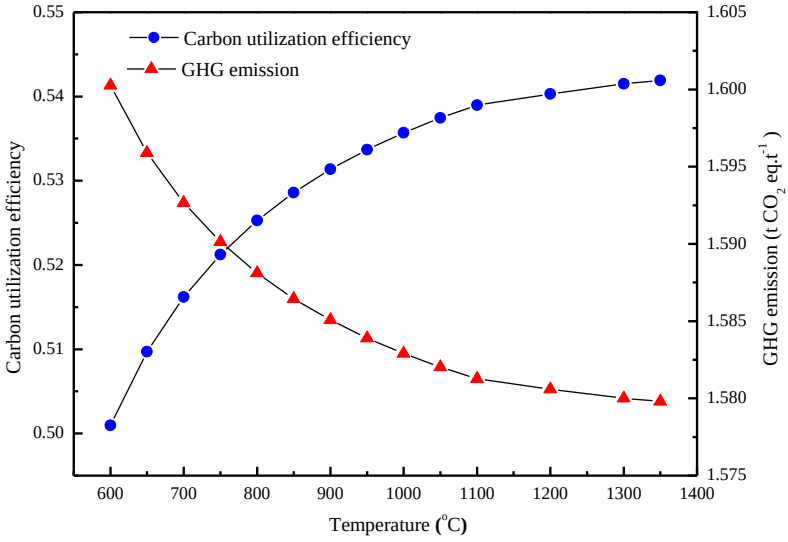

(a)

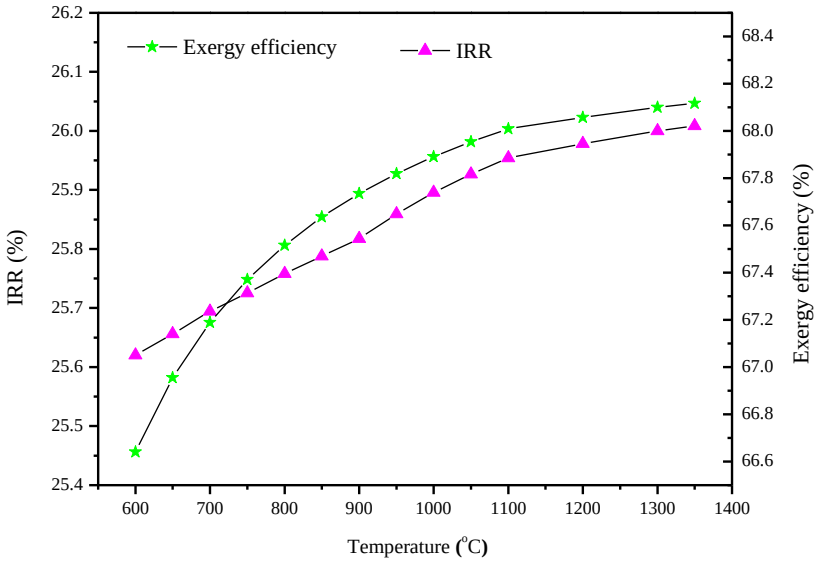

(b)

Figure S10. Effect of MPO temperature on the techno-economic performance of the system

Effect of n(O_2)/n(COG)

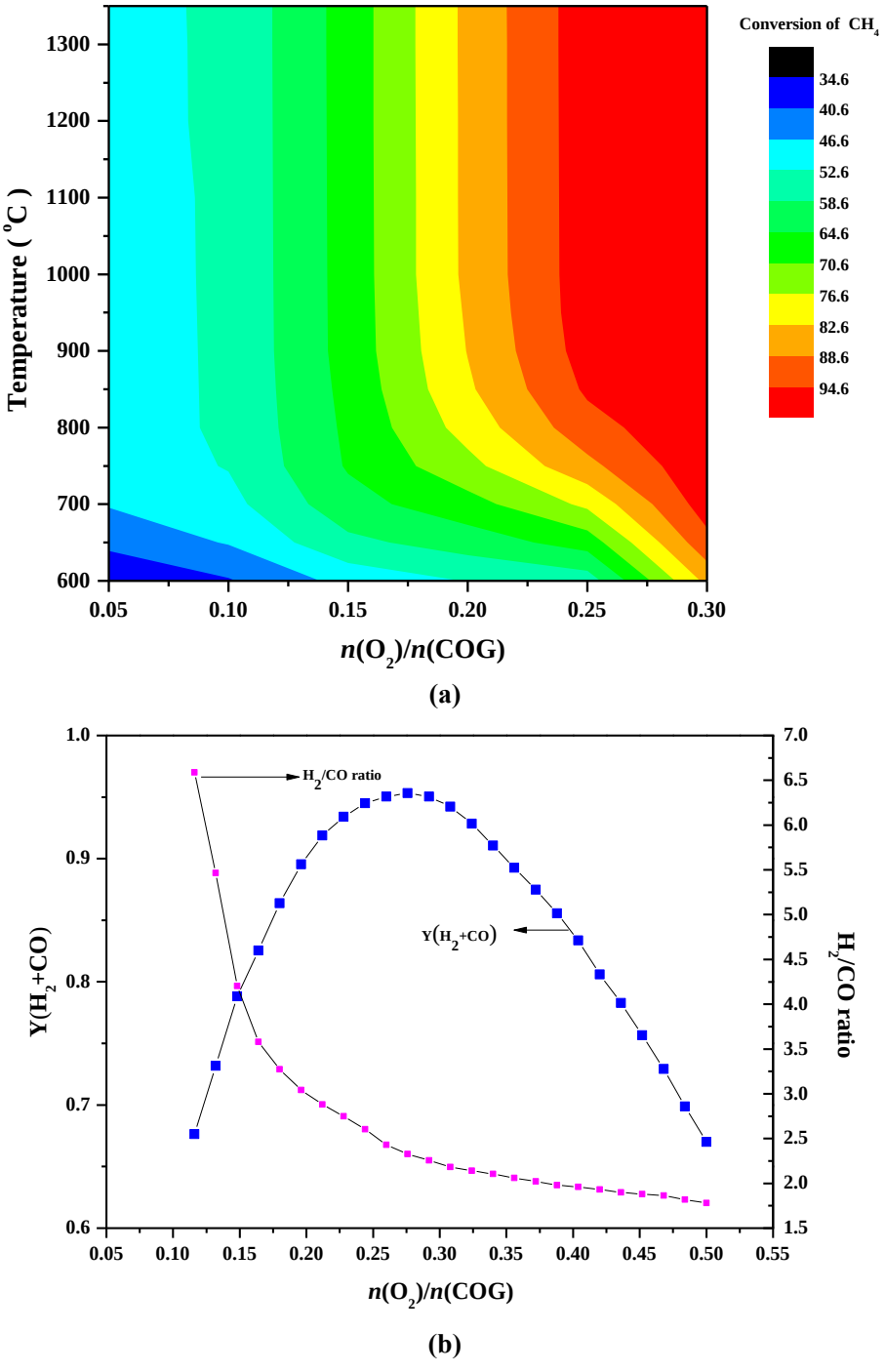

Figure S11. Effect $n(O_2)$ /n(COG) on methane conversion and H_2/CO ratio

The effect of $n(O_2)$ /n(COG)on the techno-economic performance of the system are shown in Figure S12. As the ratio of $n(O_2)$/n(COG) increased, the carbon utilization efficiency increased from 49.8% to the maximum of 54.1% and then

decreased. The GHG emissions also reduced from 1.62 t CO_2-eq.t^{-1} to the minimum of 1.58 t CO_2-eq.t^{-1}. The exergy efficiency increased from 62.3% to the peak of 68.1%. As for the economic performance, the IRR reached to maximum of 26% when the ratio of $n(O_2)/n(COG)$ is around 0.26.

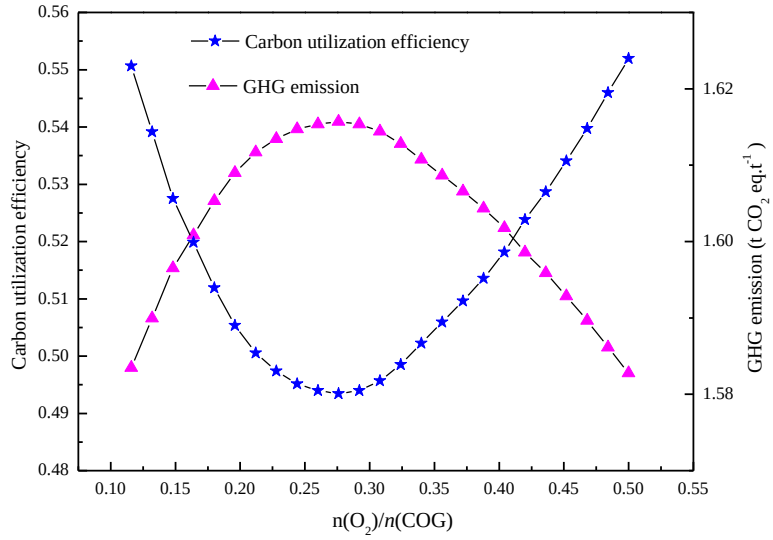

(a)

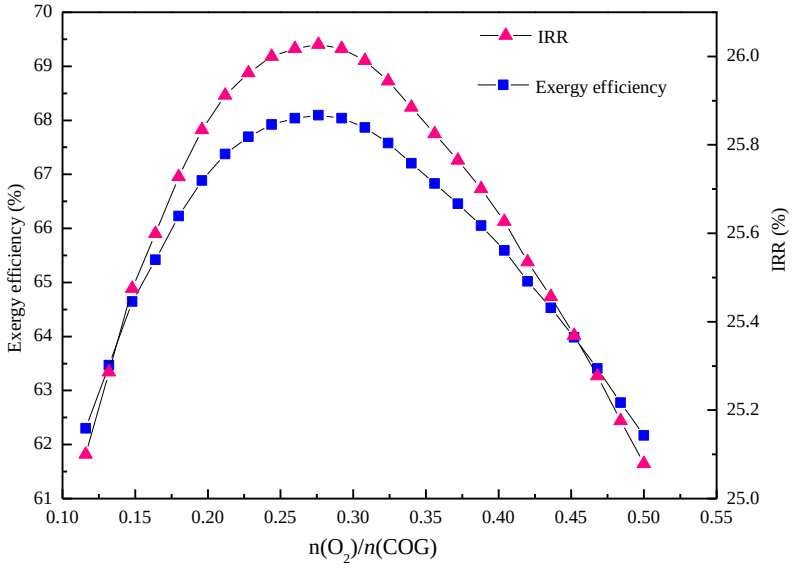

Figure S12. Effect of $n(O_2)$ /n(COG)on the techno-economic performance of the system

Key parameters analysis in MS unit

Effect of temperature and pressure

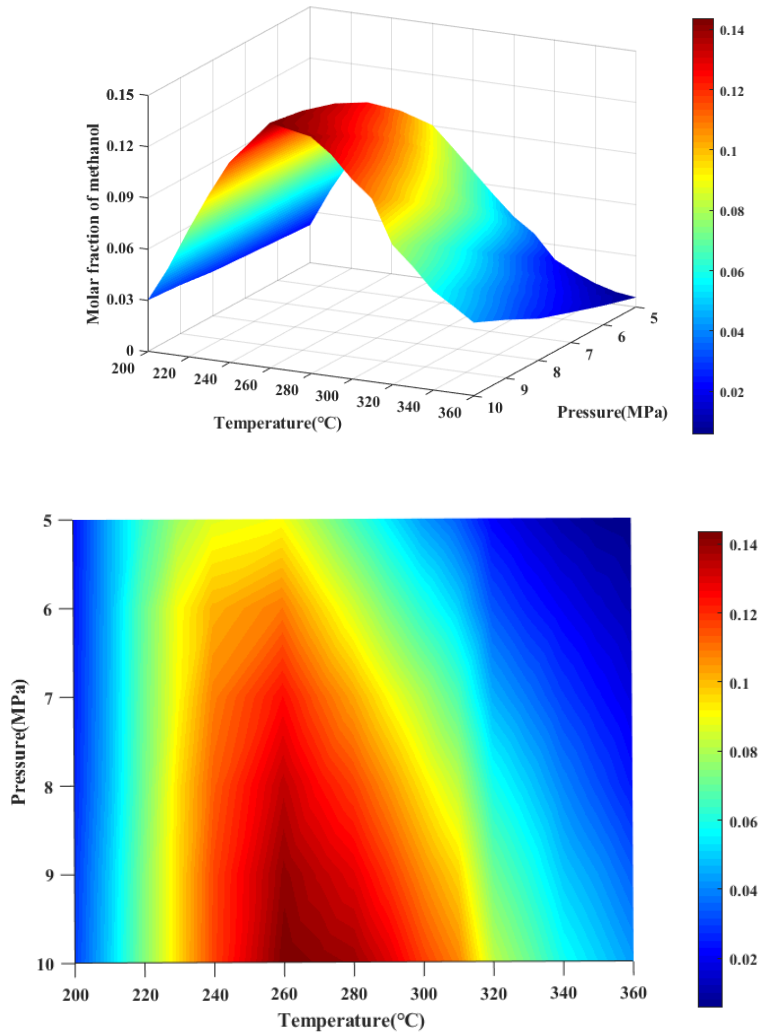

Figure S13. Effect of temperature and pressure on the methanol concentration

The effect of methanol synthesis temperature on the techno-economic performance of the system are shown in Figure S14. As the temperature increased, the carbon utilization efficiency increased from 50% to the maximum of 54% and then decreased. The GHG emissions also reduced from 1.67 t CO_2-eq.$t^{-1}$to the minimum of 1.58 t CO_2-eq.t^{-1}. The exergy efficiency increased from 64.7% to the peak of 68.1%. As for the economic performance, the IRR reached to maximum of 26% when the temperature is around 260 °C.

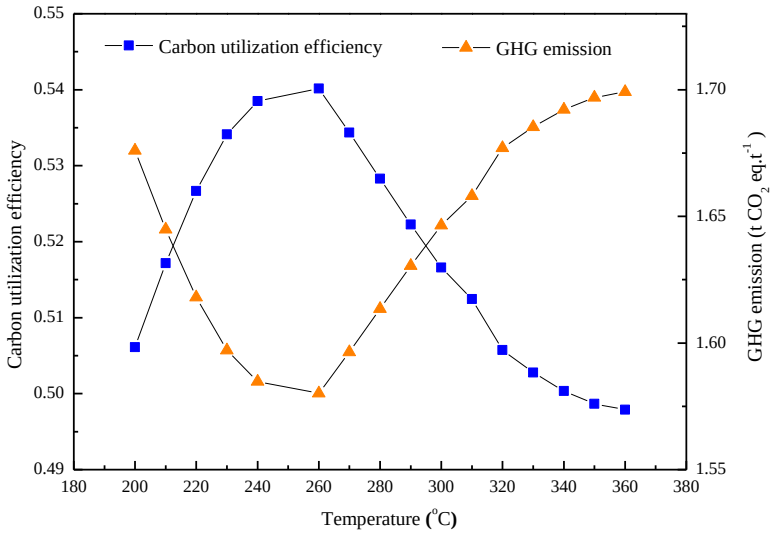

(a)

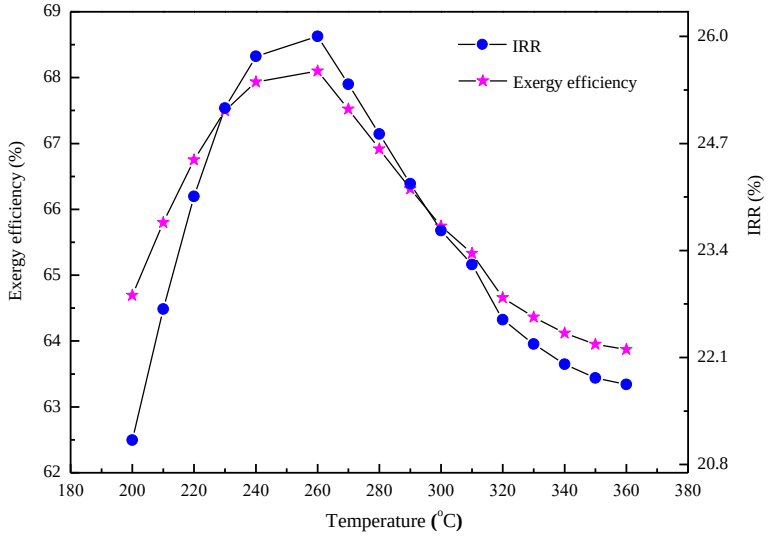

(b)

Figure S14. Effect of methanol synthesis temperature on the techno-economic performance

Effect of recycling ratio

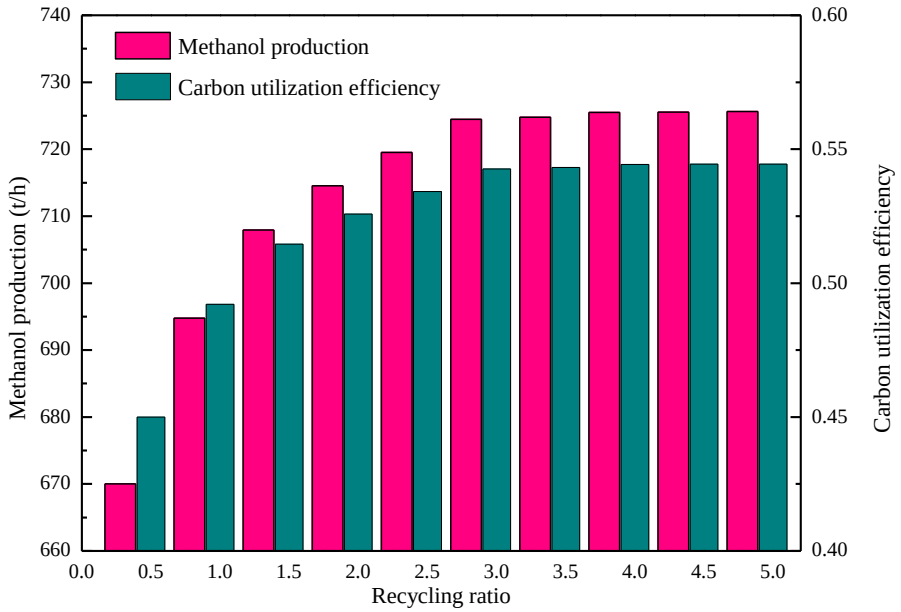

Figure S15. Effect of recycling ratio on methanol production and carbon utilization efficiency

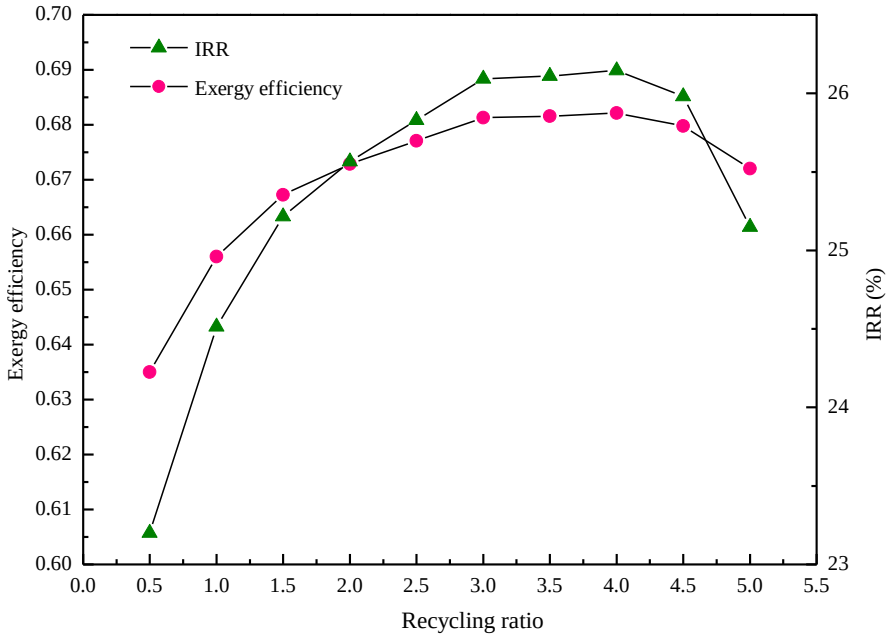

Figure S16. Effect of recycling ratio on methanol production and exergy efficiency

S5 Carbon flow diagram analysis

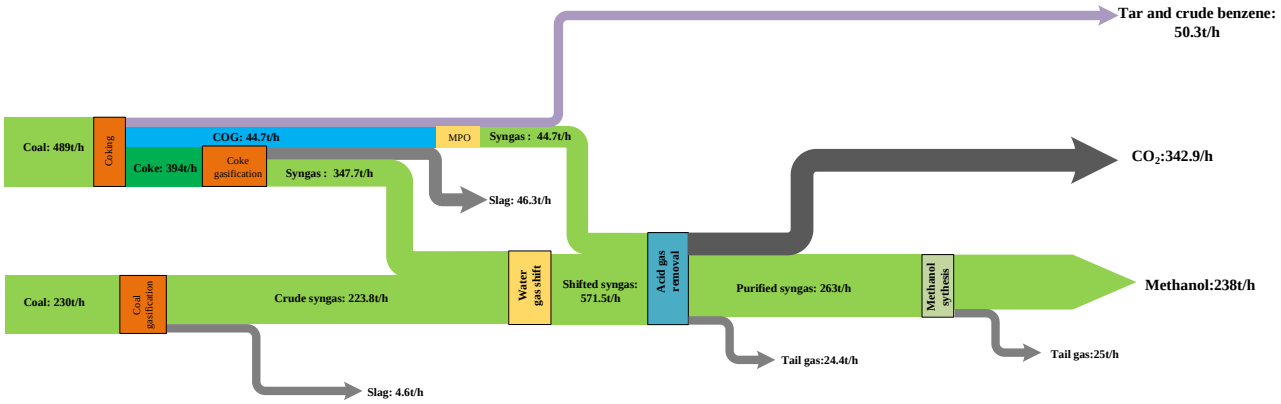

(a)

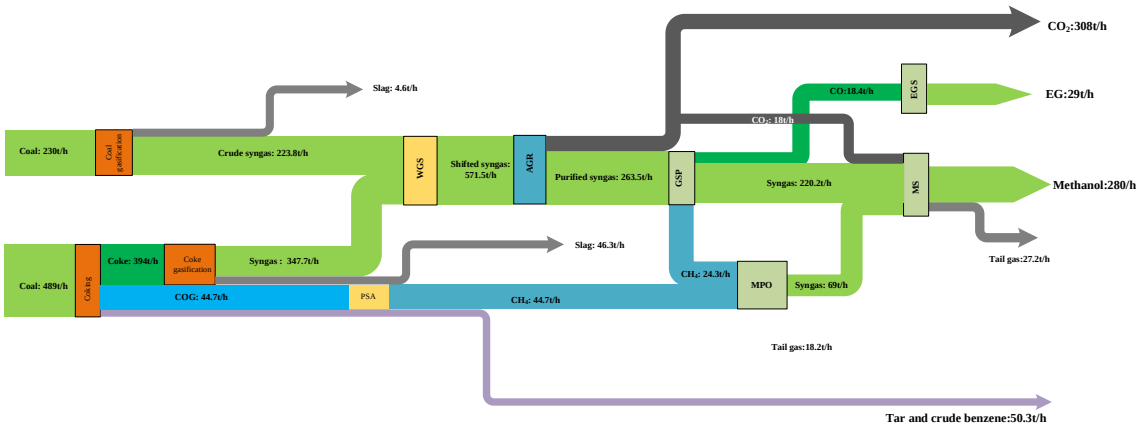

(b)

Figure S17. Carbon flow diagram of **(a)** GCtM and **(b)** GCtMEG process

References

[1] Lee, H. H.; Lee, J. C.; Joo, Y. J.; Oh, M.; Lee, C. H. Dynamic modeling of Shell entrained flow gasifier in an integrated gasification combined cycle process. *Appl. Energy* **2014**, 131, 425-440.

[2] Kong, X.; Zhong, W.; Du, W.; Qian, F. Compartment modeling of coal gasification in an

entrained flow gasifier: A study on the influence of operating conditions. *Energy Convers. Manage*. **2014**, 82, 202-211.

[3] Wan, W.; Dai, Z.; Li, C.; Yu, G.; Wang, F. Innovative concept for gasification for hydrogen based on the heat integration between water gas shift unit and coal–water–slurry gasification unit. *International J. Greenhouse Gas Con*. **2014**, 39, 7811-7818.

[4] Liu, X.; Liang, J.; Xiang, D.; Yang, S.; Qian Y. A proposed coal-to-methanol process with CO_2 capture combined Organic Rankine Cycle (ORC) for waste heat recovery. *J. Cleaner Prod*. **2016**, 129, 53-64.

[5] Lee, J. C.; Lee, H. H.; Joo, Y. J.; Lee, C. H.; Oh, M. Process simulation and thermodynamic analysis of an IGCC (integrated gasification combined cycle) plant with an entrained coal gasifier. *Energy* **2014**, 64, 58-68.

[6] Yang, S.; Qian, Y.; Ma, D.; Wang, Y.; Yang, S. BGL gasifier for coal-to-SNG: A comparative techno-economic analysis. *Energy* **2017**, 133, 158-170.

[7] Qin, S.; Chang, S.; Yao, Q. Modeling, thermodynamic and techno-economic analysis of coal-to-liquids process with different entrained flow coal gasifiers. *Appl. Energy* **2018**, 229, 413-432.

[8] Sun, L.; Smith, R. Rectisol wash process simulation and analysis. *J. Cleaner Prod*. **2013**, 39, 321-328.

[9] Liu, X.; Yang, S.; Hu, Z.; Qian, Y. Simulation and assessment of an integrated acid gas removal process with higher CO_2 capture rate. *Comput. Chem. Eng*. **2015**, 83, 48-57.

[10] Qin, S.; Chang, S. Modeling, thermodynamic and techno-economic analysis of coke production process with waste heat recovery. *Energy* **2017**, 141, 435-450.

[11] Julián, L. M.; Ortiz, A. P.; El-Halwagi, M. M.; Jiménez-Gutiérrez, A. Techno-economic assessment and environmental impact of shale gas alternatives to methanol. *ACS Sustain. Chem. Eng.* **2014**, 2, 2338-2344.

[12] Lanza, R.; Canu, P.; Järås, S. G. Methane partial oxidation over Pt–Ru catalyst: An investigation on the mechanism. Appl. *Catal A-Gen*. **2010**, 375, 92-100.

[13] Ravaghi, A. Z.; Manenti, F. Unified modeling and feasibility study of novel green pathway of biomass to methanol/dimethylether. *Appl. Energy* **2015**, *145*, 278-294.

[14] Huang, H.; Yang, S.; Cui, P. Design concept for coal-based polygeneration processes of chemicals and power with the lowest energy consumption for CO_2 capture. *Energy Convers. Manage.* **2018**, 157, 186-194.

[15] Yang, Q.; Zhang, D.; Zhou, H.; Zhang, C. Process simulation, analysis and optimization of a coal to ethylene glycol process. *Energy* **2018**, 155, 521-534.

[16] Yang, Q.; Zhang, C.; Zhang, D.; Zhou, H. Development of a coke oven gas assisted coal to ethylene glycol process for high techno-economic performance and low emission. *Ind Eng Chem. Res*. **2018**, 57, 7600-7612.

[17] Yu, B. Y.; Chien, I. L. Design and optimization of dimethyl oxalate (DMO) hydrogenation process to produce ethylene glycol (EG). *Chem. Eng. Res. Des*. **2017**, 121, 173-190.

[18] Yu, B. Y.; Chung, C. Y.; Chien, I. L. Development of a plant-wide Dimethyl Oxalate (DMO) synthesis process from syngas: Rigorous design and optimization. *Comput. Chem. Eng*. **2018**. *119,* 85-100.

[19] Peters, J. F.; Petrakopoulou, F.; Dufour, J. Exergetic analysis of a fast pyrolysis process for bio-oil production. *Fuel Process Technol*. **2014**, 119, 245-255.

[20] Morris, D. R.; Szargut, J. Standard chemical exergy of some elements and compounds on the planet earth. *Energy* **1986**, 11, 733-755.

[21] Song, G.; Xiao, J.; Zhao, H.; Shen, L. A unified correlation for estimating specific chemical exergy of solid and liquid fuels. *Energy* **2012**, 40, 164-173.